UC Berkeley

UC Berkeley Previously Published Works

Title

Structure and Function of BorB, the Type II Thioesterase from the Borrelidin Biosynthetic Gene Cluster

Permalink

https://escholarship.org/uc/item/5803h9ff

Journal

Biochemistry, 59(16)

ISSN

0006-2960

Authors

Curran, Samuel C
Pereira, Jose H
Baluyot, Marian-Joy
et al.

Publication Date

2020-04-28

DOI

10.1021/acs.biochem.0c00126

Peer reviewed

eScholarship.org Powered by the California Digital Library
University of California

Biochemistry

pubs.acs.org/biochemistry Article

Structure and Function of BorB, the Type II Thioesterase from the Borrelidin Biosynthetic Gene Cluster

Samuel C. Curran, Jose H. Pereira, Marian-Joy Baluyot, Julie Lake, Hendrik Puetz, Daniel J. Rosenburg, Paul Adams, and Jay D. Keasling*

Cite This: *Biochemistry* 2020, 59, 1630−1639 Read Online

ACCESS | Metrics & More | Article Recommendations | Supporting Information

ABSTRACT: α/β hydrolases make up a large and diverse protein superfamily. In natural product biosynthesis, *cis*-acting thioesterase α/β hydrolases can terminate biosynthetic assembly lines and release products by hydrolyzing or cyclizing the biosynthetic intermediate. Thioesterases can also act in *trans*, removing aberrant intermediates and restarting stalled biosynthesis. Knockout of this "editing" function leads to reduced product titers. The borrelidin biosynthetic gene cluster from *Streptomyces parvulus* Tü4055 contains a hitherto uncharacterized stand-alone thioesterase, *borB*. In this work, we demonstrate that purified BorB cleaves acyl substrates with a preference for propionate, which supports the hypothesis that it is also an editing thioesterase. The crystal structure of BorB shows a wedgelike hydrophobic substrate binding crevice that limits substrate length. To investigate the structure−function relationship, we made chimeric BorB variants using loop regions from characterized homologues with different specificities. BorB chimeras slightly reduced activity, arguing that the modified region is a not major determinant of substrate preference. The structure−function relationships described here contribute to the process of elimination for understanding thioesterase specificity and, ultimately, engineering and applying *trans*-acting thioesterases in biosynthetic assembly lines.

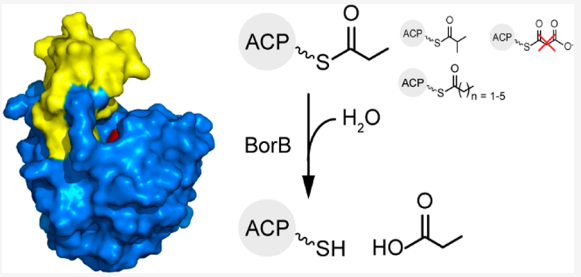

Polyketide (PK) and nonribosomal peptide (NRP) assembly line synthases utilize often-simple precursor substrates in a modular fashion to produce complex specialized metabolites. In the most simplified of these synthases, "modules", defined as the minimum unit for a chain elongation, align head to tail and pass growing intermediates between active domains via peptidyl- or acyl-carrier proteins (PCPs or ACPs, respectively). Polyketide synthases (PKSs) utilize domains that are reminiscent of fatty acid biosynthesis and catalyze a Claisen-like chain elongation and (optional) reduction.[1] Considerable diversity is installed via use of different priming and extension substrates, degree of reduction, cyclization, branching, and more.[2−4] In the type specimen for modular PKSs, the 6-deoxyerythronolide B synthase (DEBS), and many others, the final module terminates biosynthesis via a *cis*-acting thioesterase (TE) domain.[5] In DEBS, the TE catalyzes an intramolecular cyclization of the intermediate, releasing the macrocyclic product.[6]

In addition to the *cis*-TE, many biosynthetic gene clusters (BGCs) also contain a second, *trans*-acting type II TE (TEII) that operates distinctly from the biosynthetic assembly line. Knockout of TEIIs *in vivo* often leads to reduced product yields.[7] This is because TEIIs generally act as editing TEs that remove aberrant intermediates from ACPs.[7] "Dead-end" intermediates arise through several mechanisms, including the decarboxylation and protonation of malonyl-CoA and its analogues or the erroneous acyl-phosphopantetheinylation of ACPs.[8] As such, a majority of the studied TEIIs are specific for short-chain acyl substrates, such as acetyl- and propionyl-ACP.[7] However, some TEIIs play more specialized roles in starter unit control, provision of intermediates, and product release.[7] Structurally and biochemically characterized examples include the TEIIs from the tylosin,[9] FR-008,[10] coelimycin,[11] pikromycin,[12] nanchangmycin,[13] tyrocidine,[14] surfactin,[15,16] rifamycin,[17] prodigiosin,[18] and colibactin BGCs.[19]

The borrelidin polyketide cluster produces the eponymous nonaketide through the action of seven modules, terminating in a macrocyclizing TE (Figure 1).[20] The cluster also contains a putative TEII, *borB*, whose genomic knockout reduced the yield of borrelidin by 25%. To investigate BorB's biochemical activity, we characterized the purified enzyme *in vitro* with small molecule and protein substrates. We discovered that BorB readily hydrolyzes short-chain aliphatic substrates but only partially accepts longer fatty acids and diacids. Additionally, we determined the X-ray crystal structure of BorB, which reveals a canonical α/β hydrolase fold with a bifurcating

Received: February 13, 2020
Revised: April 4, 2020
Published: April 6, 2020

Downloaded via LAWRENCE BERKELEY NATL LABORATORY on August 4, 2020 at 18:16:51 (UTC).
See https://pubs.acs.org/sharingguidelines for options on how to legitimately share published articles.

ACS Publications © 2020 American Chemical Society

https://dx.doi.org/10.1021/acs.biochem.0c00126
Biochemistry 2020, 59, 1630−1639

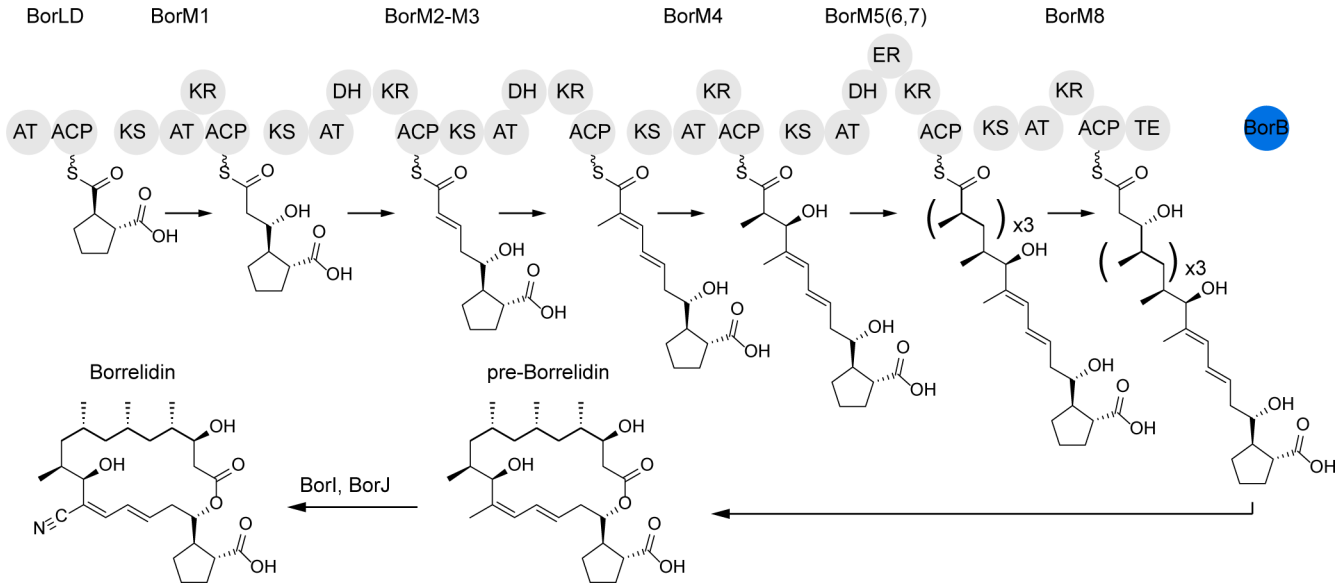

Figure 1. Borrelidin polyketide assembly line. Adapted with permission from ref 20. Copyright 2004 Elsevier.

substrate binding cleft. To investigate the structure–function relationship in BorB, we made multiple loop-swapped chimeric proteins with characterized TEIIs as donors. These chimeras displayed slightly reduced activity with a small or no shift in product preference.

MATERIALS AND METHODS

Chemical Synthesis and NMR. Synthetic procedures are detailed in the Supporting Information.

Plasmid Construction. Plasmids were designed via the J5 software package.[21] The coding sequences and backbones were prepared via polymerase chain reaction amplification with Q5 polymerase (NEB). Templates were degraded via DpnI digestion (Thermo), and the correct bands were gel extracted and assembled via Gibson assembly.[22] Assemblies were transformed into *Escherichia coli* DH10B and Sanger sequenced to verify inserts (Quintara). Physical samples and sequence maps, including primers, are available through the JBEI public registry (https://registry.jbei.org/). See the Supporting Information for detailed methods for each plasmid. Plasmids used in this study are summarized in Table S2.

Protein Purification for Biochemical Assays. BL-21 (DE3) cells containing expression plasmids were cultured overnight at 37 °C and 200 rpm in 50 mL of Terrific Broth (TB) with 50 μg/mL kanamycin before being inoculated 1% (v/v) into 2 L of TB medium with 50 μg/mL kanamycin. Cells were split into four 2 L baffled shake flasks and incubated at 37 °C and 200 rpm until the OD_{600} reached ≥0.2 AU. Protein expression was induced with 50 ng/mL anhydrotetracycline, and cells were incubated at 18 °C and 200 rpm for 20 h. Cells were centrifuged (6000*g*, 10 min, 4 °C); the supernatant was discarded, and the cells were suspended in 50 mL of lysis buffer [50 mM $NaPO_4^{2-}$ (pH 7.5), 150 mM NaCl, and 20 mM imidazole]. Cells were stirred at 200 rpm on ice until clumps were no longer visible (15–20 min). Cells were lysed by 5–10 passes through an Avestin Emulsiflex C3 homogenizer (15000 bar) and centrifuged (40000*g*, 30 min, 4 °C) to pellet the insoluble fraction.

NiNTA purification was performed using a 5 mL GE HisTrap column on an AktA explorer FPLC instrument. The column was equilibrated in 10 column volumes (CV) of lysis buffer, 10 CV of elution buffer [50 mM $NaPO_4^{2-}$ (pH 7.5), 150 mM NaCl, and 500 mM imidazole], and 10 CV of lysis buffer. The soluble fraction of the lysate was loaded onto the column via the sample pump at a rate of 2 mL/min, and the flow-through was collected. The column was washed with 10 CV of lysis buffer. The bound protein was eluted from 20 to 500 mM imidazole at a rate of 2.5 mL/min over 100 mL. The desired fractions were identified by sodium dodecyl sulfate–polyacrylamide gel electrophoresis (SDS–PAGE).

The eluent was dialyzed to remove the imidazole and salt; ~20 mL of protein from NiNTA was incubated in 1 L of AEC buffer A [50 mM $NaPO_4^{2-}$ (pH 7.5), 50 mM NaCl, and 1 mM dithiothreitol (DTT)] for 1 h at 4 °C. This process was repeated. AEC purification was performed using a 5 mL HiTrap Q anion column on an AktA explorer FPLC instrument. The column was equilibrated with 10 CV of AEC buffer A [50 mM $NaPO_4^{2-}$ (pH 7.5), 50 mM NaCl, and 1 mM DTT], 10 CV of AEC buffer B [50 mM $NaPO_4^{2-}$ (pH 7.5), 1 M NaCl, and 1 mM DTT], and an additional 10 CV of buffer A. The dialyzed protein sample was loaded via the sample pump at a rate of 5 mL/min. The bound protein was washed with 10 CV of buffer A. The bound protein was eluted in a gradient (0 to 100% buffer B over 60 min at a rate of 1 mL/min). The desired fractions were identified by SDS–PAGE.

The protein concentration in the pooled AEC fractions was quantified by UV absorbance. The sample was diluted in AEC buffer A to ~50 mM NaCl and ~2 mg/mL protein. TEV protease was added at a 1:50 molar ratio. The cleavage reaction proceeded for 16 h at 4 °C and was verified by SDS–PAGE. Subtractive NiNTA was performed as stated above with modifications. Briefly, the reaction mixture was run through an equilibrated NiNTA column at a rate of 1 mL/min and washed with an additional ~20 mL of AEC buffer A. The flow-through (cleaved protein) and eluent (tag, TEV protease, residual uncleaved protein) were collected. The purity of the flow-through was verified by SDS–PAGE (Figure S1). The flow-through was concentrated and buffer exchanged by spin filtration into 50 mM $NaPO_4^{2-}$ (pH 7.5), 8% glycerol, and 1

https://dx.doi.org/10.1021/acs.biochem.0c00126
Biochemistry 2020, 59, 1630–1639

mM DTT, flash-frozen in liquid nitrogen, and stored at −80 °C.

Kinetic Assays. Acyl-CoA kinetic assays were performed in 200 mM phosphate buffer (pH 7.6) and 0.2 mM 5,5-dithiobis(2-nitrobenzoic acid) (DTNB). The final well volume was 20 μL. Free thiol concentrations were calculated by comparison to a standard curve of *N*-acetylcysteamine (H-SNAC). The linear range under these conditions was from <5 to 250 μM. Reactions were performed in triplicate wells at 30 °C in a 384-well clear bottom plate (Thermo model 242764). Substrates were dispensed using the Echo 550 Liquid Handler. Reactions were initiated by the manual addition of 1 μM purified BorB (as shown in Figure S1), or boiled (denatured) protein serving as a negative control, to the reaction mixture. Spectrophotometric measurement at 412 nm was taken over 15 min at 30 s intervals. All wells were first background subtracted, and then rates were corrected for non-enzymatic cleavage. The linear regions of activity were used to derive kinetic constants (see the Supporting Information).

Turnover Assays. Turnover assays were performed in 200 mM phosphate buffer (pH 7.6) and 0.2 mM DTNB with 1 μM BorB and the reported substrate concentrations in 100 μL volumes. Assays were monitored continuously at 412 nm in a 96-well plate reader (SpectraMax). Absolute thiol concentrations were determined by comparison with an H-SNAC standard curve under the same conditions.

***In Vitro* ACP-acylation and MALDI-TOF.** Apo-6xHis-BorM5-ACP (50 μM) was mixed with 1 μM promiscuous *Bacillus subtilis* phosphopantetheinyltransferase SFP and 250 μM acyl-CoA and incubated at 25 °C for 1 h.[23] Samples were mixed in a 1:1 dilution series with saturated sinapinic acid in 30% H_2O and 70% acetonitrile and spotted onto a 384-well steel plate (Applied Biosystems). Samples were analyzed via an AB Sciex 4800 MALDI-TOF instrument in linear positive mode. Data were analyzed with AB Sciex Data Explorer and graphed in Python.

Size-Exclusion Chromatography−Small Angle X-ray Scattering (SEC−SAXS). BorB was prepared as stated in Protein Purification for Biochemical Assays. The final concentration of cleaved BorB was 10 mg/mL. The SEC−SAXS profile was recorded at ALS beamline 12.3.1 of the Lawrence Berkeley National Laboratory (LBNL) (X-ray wavelength λ = 1.127 Å), and the sample-to-detector distances were set to 2105 mm resulting in scattering vectors, q, ranging from 0.01 to 0.4 $Å^{-1}$.[24] The scattering vector is defined as $q = 4\pi \sin\theta/\lambda$, where 2θ is the scattering angle. All experiments were performed at 20 °C,[25] and data were processed as described previously.[26] Briefly, the flow-through SAXS cell was directly coupled with an online Agilent 1260 Infinity HPLC system using a Shodex KW-802.5 column. The column was equilibrated with running buffer [25 mM HEPES, 50 mM NaCl, 1 mM DTT, and 2% glycerol (pH 7.5)] with a flow rate of 0.55 mL/min. The 65 μL sample was run through the SEC column, and 3 s X-ray exposures were collected continuously during a 30 min elution. The SAXS frames recorded prior to the protein elution peak were used to subtract all other frames. The subtracted frames were investigated by measuring the radius of gyration (R_G) derived by the Guinier approximation $I(q) = I(0)\exp(-q^2R_G^{2/3})$ with the limits $qR_G < 1.3$. Integrals of ratios to background and R_G values were compared for each collected SAXS curve (frame) across the entire elution peak using the program SCÅTTER. The elution peak was mapped by plotting the integral of ratios to background and R_G relative to the recorded frame (Figure S6). Uniform R_G values across an elution peak represent a homogeneous sample. The merged SAXS profile was additionally investigated for aggregation using Guinier plots (Figure S7). The program SCÅTTER was used to compute the pair distribution function $P(r)$ (Figure S7). The distance r where $P(r)$ approaches zero intensity identifies the maximal dimension of the macromolecule (D_{max}). $P(r)$ functions were normalized on the basis of the molecular weight of the assemblies as determined by SCÅTTER using the volume of correlation V_c.[27] These SAXS profiles were then compared to theoretical scattering curves generated from atomistic models using FOXS.[28,29]

Protein Purification for Crystallography. The protein purification protocol detailed above was modified to use HEPES buffers. Briefly, NiNTA was performed using 25 mM HEPES (pH 7.5), 150 mM NaCl, and 20 or 500 mM imidazole. AEC buffers consisted of 25 mM HEPES (pH 7.5), 1 mM DTT, and either 50 mM or 1 M NaCl. BorB was cleaved and purified from its MBP tag as described. The cleaved sample was concentrated to 10 mg/mL by spin filtration and immediately distributed in crystallization trays.

Crystallization, X-ray Data Collection, and Structure Determination. The BorB protein was screened using the sparse matrix method[30] with a Phoenix Robot (Art Robbins Instruments, Sunnyvale, CA) using the following crystallization screens: Berkeley Screen,[31] Crystal Screen, SaltRx, PEG/Ion, Index, and PEGRx (Hampton Research, Aliso Viejo, CA). Crystals of BorB were found in 0.2 M MgCl, 0.1 M HEPES (pH 7.5), and 22% poly(acrylic acid sodium salt) 5100. BorB crystals were obtained by the sitting-drop vapor-diffusion method with the drops consisting of a mixture of 0.2 μL of a protein solution and 0.2 μL of a reservoir solution. A crystal of BorB was placed in a reservoir solution containing 20% (v/v) glycerol and then flash-cooled in liquid nitrogen. The X-ray data sets for BorB were collected at Berkeley Center for Structural Biology beamline 8.2.2 of the Advanced Light Source at LBNL. The diffraction data were recorded using an ADSC-Q315r detector. The data sets were processed using the program Xia2.[32]

The BorB crystal structure was determined by the molecular-replacement method with the program PHASER[33] within the Phenix suite[34,35] using as a search model the structure of TEII RifR [Protein Data Bank (PDB) entry 3FLA],[17] which was 50% identical to the sequence of the target. The atomic positions obtained from molecular replacement and the resulting electron density maps were used to build the BorB structure and initiate crystallographic refinement and model rebuilding. Structure refinement was performed using the phenix.refine program.[35] Translation−libration−screw (TLS) refinement was used, with each protein chain assigned to a separate TLS group. Manual rebuilding using COOT[36] and the addition of water molecules allowed construction of the final model. The final model of BorB has an R factor of 23.3% and an R_{free} of 26.9%. Root-mean-square deviations from ideal geometries for bond lengths, angles, and dihedrals were calculated with Phenix.[34] The stereochemical quality of the final model of BorB was assessed with the program MOLPROBITY.[37] Crystallization parameters are listed in Table 1.

RESULTS

BorB Is a TEII. BorB clades with the TE18 family of α/β hydrolases from PKSs and NRPSs based on primary sequence

https://dx.doi.org/10.1021/acs.biochem.0c00126
Biochemistry 2020, 59, 1630−1639

Table 1. Statistics for X-ray Data Collection and Structure Refinement of BorB

(A) Data Collection	
wavelength (Å)	0.99998
resolution range (Å)	39.33−1.93 (1.99−1.93)
detector distance (mm)	220
Φ (deg) collected/ΔΦ (deg)	200/1.0
exposure time (s)	3
collection temperature (K)	100
(B) Data Statistics	
space group	*C*2221
unit cell parameters (Å)	a = 72.45, b = 92.36, c = 150.14
total no. of reflections	303622 (30958)
no. of unique reflections	37964 (3740)
multiplicity	8.0 (8.3)
data completeness (%)	99.19 (99.02)
mean $I/\sigma(I)$	15.18 (1.46)
Wilson *B*-factor	27.26
R_{merge}	0.1059 (1.601)
R_{meas}	0.1133 (1.705)
R_{pim}	0.03964 (0.5825)
$CC_{1/2}$	0.999 (0.667)
CC*	1 (0.895)
(C) Structure Refinement	
no. of reflections used in refinement	37936 (3737)
no. of reflections used for R_{free}	1883 (183)
R_{work}	0.2085 (0.3639)
R_{free}	0.2498 (0.4547)
CC(work)	0.948 (0.790)
CC(free)	0.940 (0.556)
RMSD from ideal geometry	
bond lengths (Å)	0.011
bond angles (deg)	0.91
no. of protein residues	480
no. of water molecules	367
average isotropic *B*-factor (Å^2)	
protein atoms	39.86
solvent atoms	39.75
Ramachandran plot (%)	
favored region	97.89
outlier region	0.2
rotamer outliers	0.26
Clashscore	4.3
MolProbity score	1.24

alignment.[38] Alignment of more than 200 putative and well-studied TEIIs, such as RifR and RedJ, revealed a classic catalytic triad of S98, D204, and H232 (numbering based on our cleaved expression construct) (see the Supporting Information). To confirm BorB's thioesterase activity, we expressed codon-optimized BorB in *E. coli*. We could detect soluble BorB only when it was expressed as an N-terminal hexahistidine maltose binding protein (MBP) fusion.[39] 6xHis-MBP-TEV-BorB was purified, and BorB was cleaved from the His-MBP tag (Figure S1). Cleaved BorB was reacted with synthesized acyl-*N*-acetylcysteamine thioesters (SNACs), well-established substrate analogues for PKSs and TEIIs (see the Supporting Information for synthetic details).[40] We continuously monitored thioester cleavage via colorimetric Ellman's assays (Figure S2).[41] BorB readily cleaved acetyl- and hexanoyl-SNAC, and the activity was linearly dependent on both time and enzyme concentration (Figure S3). To verify that specifically BorB, and not a co-eluent, was responsible for the observed cleavage, we mutated the catalytic serine to an alanine. This mutant, BorB S98A, had no detectable activity when purified and reacted with acetyl-SNAC (Figure S4).

BorB Substrate Specificity. To investigate BorB's substrate preference, we performed Michaelis−Menten kinetic assays with aliphatic acyl-CoA substrates (Figure 2). We used

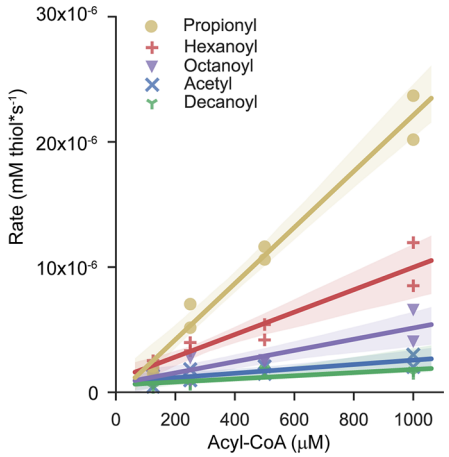

Figure 2. Kinetic assays of BorB with acyl-CoAs.

the linear region of rate curves to estimate k_{cat}/k_m (see Materials and Methods). BorB had the highest activity on propionyl-CoA (k_{cat}/k_m = 22.4 ± 3.5 M^{-1} s^{-1}), followed by hexanoyl-CoA (k_{cat}/k_m = 8.9 ± 3.1 M^{-1} s^{-1}) (Table 2). After

Table 2. Kinetic Parameters for BorB[a]

acyl-CoA	k_{cat}/k_m (M^{-1} s^{-1})
acetyl	1.7 ± 1.3
decanoyl	1.2 ± 1.0
hexanoyl	8.9 ± 3.1
octanoyl	4.5 ± 2.5
propionyl	22.4 ± 3.5
palmitoyl	BD
malonyl	BD
methylmalonyl	BD
succinyl	BD
adipyl	BD
3-hydroxybutyryl	BD
isobutyryl	BD

[a]BD, below detection. N = 2 experiments, performed in technical triplicate on separate days.

hexanoyl-CoA, activity correlated inversely with chain length; octanoyl- and decanoyl-CoA were cleaved with k_{cat}/k_m values of 4.5 ± 2.5 and 1.2 ± 1.0 M^{-1} s^{-1}, respectively (Table 2). BorB had low activity (1.7 ± 1.3 M^{-1} s^{-1}) on acetyl-CoA (Table 2). We did not detect thioester cleavage above background for palmitoyl-CoA, isobutyryl-CoA, 3-hydroxybutyryl-CoA, and diacids malonyl-, methylmalonyl-, succinyl-, and adipyl-CoA at concentrations of 2 mM (Figure S5).

As TEIIs generally interact with ACPs and PCPs of biosynthetic assembly lines, the probable native substrate of BorB is an acyl-ACP.[7] To test if BorB cleaved acyl-ACPs, we expressed and purified the apo-ACP from the fifth module of the borrelidin synthase (BorM5-ACP). BorM5-ACP was phosphopantetheinylated *in vitro* and reacted with BorB

https://dx.doi.org/10.1021/acs.biochem.0c00126
Biochemistry 2020, 59, 1630−1639

(Figure 3A). Acyl-ACP cleavage was assessed by matrix-assisted laser desorption time-of-flight mass spectrometry

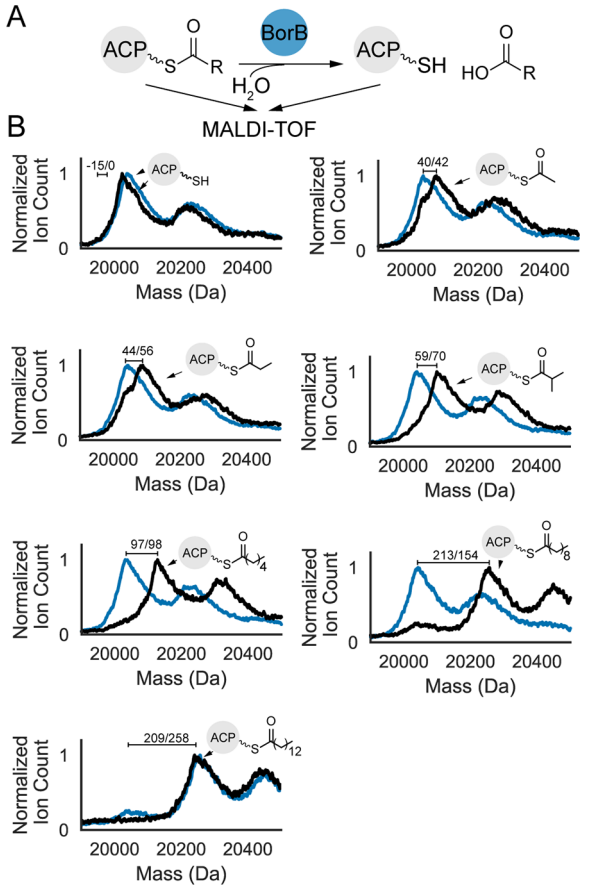

Figure 3. MALDI-TOF MS of acyl-ACP with BorB. (A) Experimental scheme for detection of ACP cleavage by MALDI-TOF MS. (B) MALDI-TOF MS chromatograms of acyl-BorACP5 without BorB (black) and with 1 mM BorB (blue). ACPs are indicated in each subplot. Peak shifts between acyl- and holo-ACP are denoted with observed/expected mass shifts.

(MALDI-TOF MS). Despite the rather poor mass resolution, we observed clear peak shifts from holo-acyl-ACP to acyl-ACPs ranging from C_2 to C_{14} (Figure 3B). After incubation with BorB for 1 h, we observed cleavage of acyl-BorM5-ACP with chains up to and including decanoyl (C_{10}). We observed minimal cleavage of myristoyl-ACP5 (C_{14}).

Overall Structure of BorB. The crystal structure of BorB was determined at 1.93 Å resolution, revealing an α/β hydrolase fold (Figure 4A).[42] Two molecules of BorB formed the asymmetric unit (Figure S8). However, BorB lacks the N-terminal helices reported to be important for dimerization in the Pik and DEBS TEs (Figure S9).[43] To confirm BorB's quaternary state, we performed size-exclusion chromatography coupled to small angle X-ray scattering (SEC−SAXS). The scattering curve shows a monomeric globular protein with a radius of gyration (R_G) of 19 Å and a D_{max} of 64 Å (Table S1). Back-calculation of scattering curves was performed using the FOXS server.[28,29] The in solution data are clearly more consistent with those of monomeric BorB than those of dimeric BorB ($\chi_{monomer}^2$ = 1.08; χ_{dimer}^2 = 19.85) (Figure S10).

BorB forms a two-lobed structure with an α/β hydrolase core and a "lid region" (Figure 4A). BorB has seven β-strands (2−8) and lacks strand β1, similar to other PKS TEs (Figure 4C).[6] The core begins with a pair of antiparallel β-strands (β2−β4) and continues with alternating α-helices and β-strands. The lid region, while found commonly in α/β hydrolases, contributes significantly to their structural variability.[44] In BorB and other monomeric TEs, the lid extends between strands β6 and β7 (Figure 4C).[6] BorB's lid is formed from three α-helices (αL1−αL3, residues 138−183). The two BorB molecules found in the asymmetric unit show the largest difference in the lid region. Chain B contains an intact lid, while chain A lacks electron density for the C-terminal half of αL2 (Figure 3B). Upon comparison of chains A and B, the lid region shows an $RMSD_{Lid}$ of 2.075 Å while the core region an $RMSD_{Core}$ of 1.178 Å. These distinct forms of the lid region, dubbed "Open" and "Closed" conformations, have been captured in numerous TE structures.[17−19,45,46] The lid and its associated flexible loops likely control the accessibility of the substrate binding chamber to acyl-ACPs via an N-terminal ACP entrance. In BorB's Open configuration, the catalytic cleft is accessible from both sides. In the Closed configuration, the N-terminal ACP entrance is obstructed by αL2 of the lid. Additionally, the lid shows considerable flexibility in both chains. The *B*-factor values, which indicate chain flexibility, are highest between lid helices αL2 and αL3 (Figure S11).

Active Site of the BorB Structure. The lid and its associated flexible loops determine the size, shape, and presumably substrate binding preference of the chamber. In the macrocyclizing TEs from the pikromycin and DEBS synthases, the substrate channel penetrates through the enzyme, forming a donutlike aperture that favors macrocyclization.[43,47] In contrast, the substrate channel in BorB resembles a wedgelike crevice that is also found in many noncyclizing TEs (Figure 4A).[17−19,46] The catalytic serine sits in the canonical G96-H97-S98-X99-G100 motif after strand β5. This residue is positioned in a hairpin loop at the N-terminus of helix αC. This "nucleophilic elbow" is typical of α/β hydrolases.[44] The other members of the catalytic triad, D204 and H232, sit after strands β7 and β8, respectively, and are hydrogen bonded. The backbone amide of A33 forms the putative oxyanion hole.[17]

BorB Substrate Binding Site. Numerous BorB homologues have been modeled or co-crystallized with substrates, nonhydrolyzable analogues, and ACPs (Figure S12). Studies of the DEBS TE identified an arginine-rich patch on the N-terminal half of the protein, to which the ACP was computationally docked.[43] Structures of the surfactin TE with bound peptides,[45] hFAS TE with polyunsaturated fatty acids,[48] and the pikromycin TE with nonhydrolyzable substrate analogues,[49] co-crystallization of the NRPS enterocin thioesterase EntF with apo-[50−52] and crypto-ACP,[50−52] and co-crystallization of the valinomycin TE Vlm2 with peptide intermediates support this model[52] and lead to a putative chamber for the acyl substrate where the acyl-ACP enters from the right side of the crevice (Figure S13). The substrate binding chamber therefore likely lays to the left of S98 when facing the binding cleft.

In BorB, the front of this putative binding chamber is bounded by "catalytic loops" 1 and 2, which contain the catalytic D204 and H232, respectively (Figure 5A). Catalytic loop 2 is highly conserved (Figure S14), while catalytic loop 1 contains considerable diversity apart from catalytic D204 (Figure S14). The binding pocket is largely hydrophobic proximal to S98, with contributions from residues M99, A33,

https://dx.doi.org/10.1021/acs.biochem.0c00126
Biochemistry 2020, 59, 1630−1639

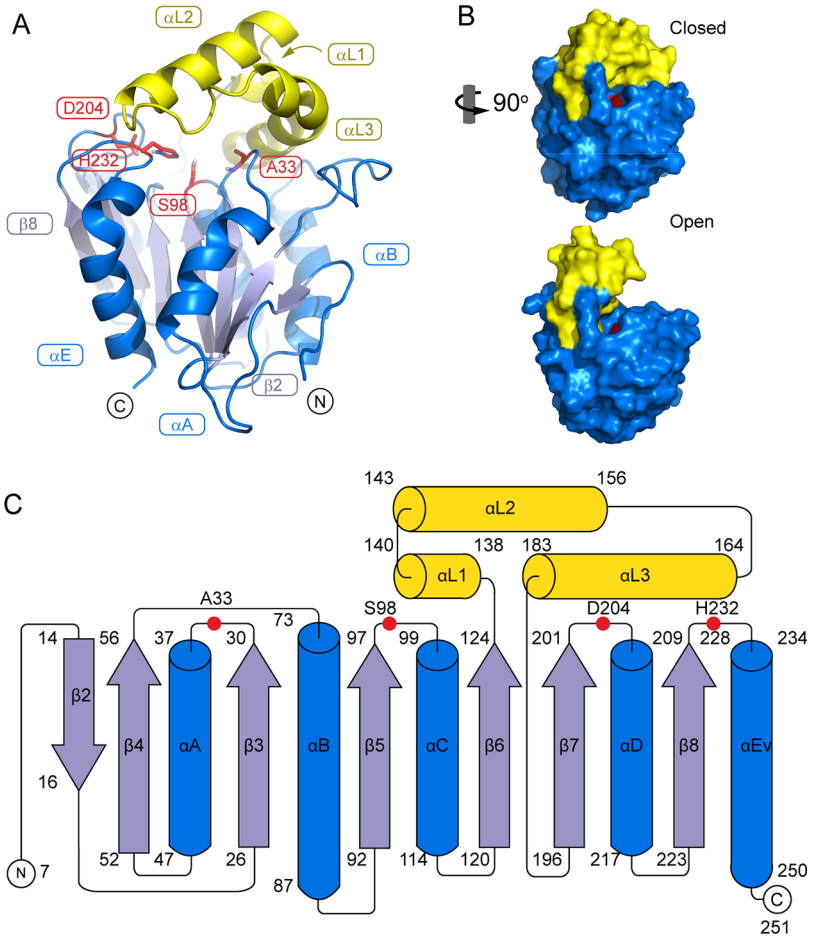

Figure 4. Overall structure of BorB. (A) Overlaid structures of chains A and B of BorB. Lid regions are colored orange and yellow, respectively. The active triad is colored red. (B) Individual monomers of the asymmetric unit. The coloring is identical to that of panel A. (C) Topology diagram of BorB.

and A181 (Figure S15). The pocket bifurcates toward the "exit" of the tunnel. The top and back boundaries are formed by helices αL2 and αL3, respectively (Figure 5A). In the long-chain hydrolyzing RedJ, this pocket is lined with short hydrophobic residues and one form of RedJ was co-crystallized with PEG in the crevice.[18] However, in the promiscuous TEII RifR, this pocket is occluded by bulky, polar residues.[17] Similarly, this pocket in BorB is filled with polar residues E182, Y178, and E149. Y178 forms the roof of the binding pocket. Lid loop 1 and helix αL1 form the left wall of the pocket (Figure 5A). This wall consists of 20−30 poorly conserved residues bounded by conserved serine and aspartate residues (S124 and D143, respectively) (Figure 5B). R126 forms the border of the hydrophobic pocket proximal to S98, suggesting it may be involved in substrate preference (Figure 5A).

Engineering BorB. Chain release can be an important control point in engineered polyketide systems.[53] Thus, we endeavored to engineer BorB to accept longer substrates. Lid loop 1 has been proposed to control substrate preference in several TEs.[18,19,46] To investigate this possibility, we generated chimeric swaps with characterized TEIIs RifR, RedJ, and ScoT.[11,17,18] RedJ prefers C_{10}−C_{12} esters; RifR is promiscuous, and ScoT prefers propionate esters. RifR and RedJ have been structurally characterized. All four proteins contain lid loop 1 (Figure 5C) and differ considerably in this region (Figure S16). RedJ contains a serine in place of R126, allowing us to test whether this residue limits the length of nonpolar substrates. The chimeras were expressed in and purified from *E. coli*. BorB-RifR and BorB-ScoT had roughly 25% yield of WT BorB, indicating instability and degradation. These proteins were assayed for altered activity on acyl-CoAs using Ellman's assay (Figure 5D). Donor loops from ScoT and RedJ lead to an ∼30% loss of activity on propionyl-CoA, while the loop from RifR leads to a 75% loss of activity. BorB-RifR and RedJ mutants exhibited a modest 2−4-fold increase in activity with acetyl-CoA. No mutants had improved activity on hexanoyl- or decanoyl-CoA.

DISCUSSION

BorB's broad substrate preference, and the fact that it improves but is not required for borrelidin biosynthesis, suggests that it is an editing TEII.[20] Of the acyl-CoAs tested, BorB exhibited the highest activity on propionyl-CoA. BorB exhibited a similar pattern with acyl-ACPs; BorB was active on short-chain acyl-BorACP5, but its activity dropped off with an increase in chain length. Propionyl-ACP can arise from the decarboxylation of methylmalonyl-ACP and aberrant protonation, rather than condensation with the priming unit. In borrelidin biosynthesis, modules BorM3−BorM5 utilize methylmalonyl-CoA and may therefore be targets of BorB (Figure 1).[20]

A bifurcating substrate pocket in BorB permits aliphatic substrates and supports the preference for the propionyl-

https://dx.doi.org/10.1021/acs.biochem.0c00126
Biochemistry 2020, 59, 1630−1639

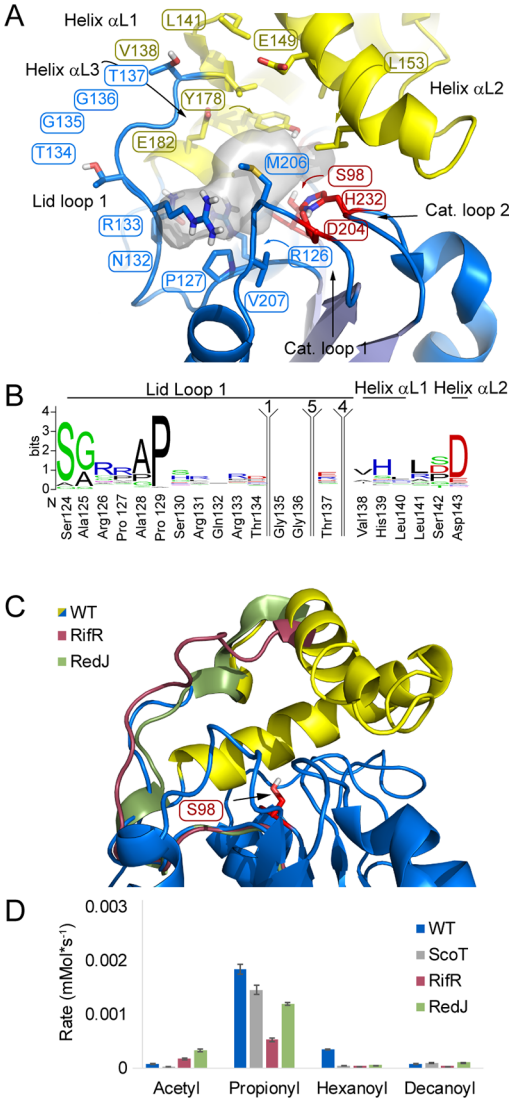

Figure 5. Engineering BorB for an altered substrate profile. (A) Active site of BorB. The cavity is shown with a gray surface. (B) Conservation of the region used to generate chimeric proteins. Larger letters indicate higher degrees of conservation. Collapsed regions are indicated by the number of amino acids and are not present in BorB. G135 and G136 are unique to BorB. (C) Overlay of chain B of BorB with the structures of RifR (PDB entry 3FLA) and RedJ (PDB entry 3QMW). The swapped loop regions are colored. (D) Acyl-CoA hydrolysis assay of WT and chimeric BorB variants. Error bars are standard deviations of technical duplicates.

thioester. To understand the structure−function relationship of BorB, we targeted one arm of the binding pocket using loop swaps with well-characterized TEIIs. Chimeric proteins have had some success in altering product profiles in the TE14 family of hotdog fold TEs.[54] However, the chimeras made here did not lead to major changes in specificity, and ∼70% of the activity was preserved with donors from ScoT and RedJ. Thus, lid loop 1 may be too distant from the binding site to directly affect substrate preference. Minor alterations in substrate specificity may be due to lid loop 1's involvement in binding crevice flexibility.[17] Thus, future efforts may yield greater success by focusing on different regions of the binding pocket. The region between helices αL2 and αL3 and not lid loop 1 may be the differentiating factor.[18] E149 and Y178 stand out as residues that are highly conserved in editing TEIIs but are replaced by valine and leucine, respectively, in the long-chain specific TEII RedJ (Figure S17). These substitutions may open this arm of the pocket for longer aliphatic substrates.

α/β hydrolases such as esterases or lipases are among the most successfully engineered proteins and are often used to validate high-throughput enzyme engineering strategies.[55] However, to the best of our knowledge, this success has not been translated to PKS and NRPS TEs.[56] Rational site-directed mutagenesis of the substrate pockets of PKS and NRPS TEs often leads to diminution of activity.[18,57,58] This challenge is complicated by the movement of residues and subdomains throughout catalysis.[52,59] In addiiton, *in silico* prediction of TE specificity is currently not possible,[6] as TEs cluster by biosynthetic class, i.e., PKS versus NRPS, rather than substrate specificity.[60]

CONCLUSIONS

A large library of characterized TEs may prove to be necessary for dissecting this complex relationship. Here we provide a kinetic and structural characterization of the editing TEII BorB, explaining its auxiliary role in borrelidin biosynthesis. These findings contribute to the process of elimination in identifying the structural determinants of TE substrate specificity.

ASSOCIATED CONTENT

Supporting Information

The Supporting Information is available free of charge at https://pubs.acs.org/doi/10.1021/acs.biochem.0c00126.

Supporting data and methods (PDF)

Accession Codes

BorB: Uniprot, Q70I09; PDB, 6VAP.

AUTHOR INFORMATION

Corresponding Author

Jay D. Keasling − *Joint BioEnergy Institute, Emeryville, California 94608, United States; Biological Systems & Engineering Division, Lawrence Berkeley National Laboratory, Berkeley, California 94720, United States; Department of Bioengineering and Department of Chemical & Biomolecular Engineering, University of California, Berkeley, Berkeley, California 94720, United States*; Email: jdkeasling@lbl.gov

Authors

Samuel C. Curran − *Comparative Biochemistry Graduate Group, University of California, Berkeley, Berkeley, California 94720, United States; Joint BioEnergy Institute, Emeryville, California 94608, United States;* orcid.org/0000-0001-7748-5374

Jose H. Pereira − *Joint BioEnergy Institute, Emeryville, California 94608, United States; Biological Systems & Engineering Division, Lawrence Berkeley National Laboratory, Berkeley, California 94720, United States*

Marian-Joy Baluyot − *Joint BioEnergy Institute, Emeryville, California 94608, United States; Department of Molecular and Cell Biology, University of California, Berkeley, Berkeley, California 94720, United States*

Julie Lake − *Joint BioEnergy Institute, Emeryville, California 94608, United States; Department of Plant and Microbial Biology, University of California, Berkeley, Berkeley, California 94720, United States*

https://dx.doi.org/10.1021/acs.biochem.0c00126
Biochemistry 2020, 59, 1630−1639

Hendrik Puetz − *Joint BioEnergy Institute, Emeryville, California 94608, United States; Department of Biochemistry, University of Cologne, Cologne 51149, Germany*

Daniel J. Rosenburg − *Graduate Group in Biophysics, University of California, Berkeley, Berkeley, California 94720, United States; Molecular Biophysics and Integrated Bioimaging, Lawrence Berkeley National Laboratory, Berkeley, California 94720, United States*

Paul Adams − *Joint BioEnergy Institute, Emeryville, California 94608, United States; Molecular Biophysics and Integrated Bioimaging, Lawrence Berkeley National Laboratory, Berkeley, California 94720, United States; Department of Bioengineering, University of California, Berkeley, Berkeley, California 94720, United States*

Complete contact information is available at: https://pubs.acs.org/10.1021/acs.biochem.0c00126

Author Contributions

S.C.C. designed and performed experiments. J.H.P. performed crystallography experiments and determined structures. M.-J.B., J.L., and H.P. performed cloning and enzyme activity experiments. D.J.R. performed SEC−SAXS analysis. P.A. and J.D.K. provided mentorship and experimental guidance. S.C.C. wrote the manuscript with input from all authors.

Funding

This work was performed at the DOE Joint BioEnergy Institute (http://www.jbei.org), which is supported by the U.S. Department of Energy, Office of Science, Office of Biological and Environmental Research, through Contract DE-AC02-05CH11231 between Lawrence Berkeley National Laboratory and the U.S. Department of Energy. This research was also conducted as part of the Co-Optimization of Fuels & Engines (Co-Optima) project sponsored by the U.S. Department of Energy (DOE) Office of Energy Efficiency and Renewable Energy (EERE), Bioenergy Technologies and Vehicle Technologies Offices. Crystallography experiments were performed at beamline 8.2.2 of the Advanced Light Source (ALS), a DOE Office of Science User Facility under Contract DE-AC02-05CH11231, and were supported in part by the ALS-ENABLE program funded by the National Institutes of Health, National Institute of General Medical Sciences, via Grant P30 GM124169-01. SEC−SAXS experiments were conducted at the ALS through the Integrated Diffraction Analysis Technologies (IDAT) program, supported by DOE Office of Biological and Environmental Research. Additional support comes from the National Institute of Health Project ALS-ENABLE (P30 GM124169) and a High-End Instrumentation Grant (S10OD018483).

Notes

The authors declare the following competing financial interest(s): J.D.K. has financial intertest in Amyris, Lygos, Demetrix, Maple Biotechnology, Napigen, Ansa Biotechnology, and Apertor Laboratories.

■ ACKNOWLEDGMENTS

Jacquelyn Blake-Hedges provided purified SFP. pRK793 was a gift from D. Waugh. The authors thank the College of Chemistry's NMR facility for resources provided and the staff for their assistance.

■ REFERENCES

(1) Keatinge-Clay, A. T. (2012) The structures of type I polyketide synthases. *Nat. Prod. Rep. 29*, 1050−1073.
(2) Keatinge-Clay, A. T. (2017) The Uncommon Enzymology of Cis-Acyltransferase Assembly Lines. *Chem. Rev. 117*, 5334−5366.
(3) Hertweck, C. (2009) The biosynthetic logic of polyketide diversity. *Angew. Chem., Int. Ed. 48*, 4688−4716.
(4) Sundaram, S., and Hertweck, C. (2016) On-line enzymatic tailoring of polyketides and peptides in thiotemplate systems. *Curr. Opin. Chem. Biol. 31*, 82−94.
(5) Khosla, C., Herschlag, D., Cane, D. E., and Walsh, C. T. (2014) Assembly line polyketide synthases: mechanistic insights and unsolved problems. *Biochemistry 53*, 2875−2883.
(6) Horsman, M. E., Hari, T. P. A., and Boddy, C. N. (2016) Polyketide synthase and non-ribosomal peptide synthetase thioesterase selectivity: logic gate or a victim of fate? *Nat. Prod. Rep. 33*, 183−202.
(7) Kotowska, M., and Pawlik, K. (2014) Roles of type II thioesterases and their application for secondary metabolite yield improvement. *Appl. Microbiol. Biotechnol. 98*, 7735−7746.
(8) Walsh, C. T., Gehring, A. M., Weinreb, P. H., Quadri, L. E., and Flugel, R. S. (1997) Post-translational modification of polyketide and nonribosomal peptide synthases. *Curr. Opin. Chem. Biol. 1*, 309−315.
(9) Heathcote, M. L., Staunton, J., and Leadlay, P. F. (2001) Role of type II thioesterases: evidence for removal of short acyl chains produced by aberrant decarboxylation of chain extender units. *Chem. Biol. 8*, 207−220.
(10) Zhou, Y., Meng, Q., You, D., Li, J., Chen, S., Ding, D., Zhou, X., Zhou, H., Bai, L., and Deng, Z. (2008) Selective removal of aberrant extender units by a type II thioesterase for efficient FR-008/candicidin biosynthesis in Streptomyces sp. strain FR-008. *Appl. Environ. Microbiol. 74*, 7235−7242.
(11) Kotowska, M., Pawlik, K., Smulczyk-Krawczyszyn, A., Bartosz-Bechowski, H., and Kuczek, K. (2009) Type II thioesterase ScoT, associated with Streptomyces coelicolor A3(2) modular polyketide synthase Cpk, hydrolyzes acyl residues and has a preference for propionate. *Appl. Environ. Microbiol. 75*, 887−896.
(12) Kim, B. S., Cropp, T. A., Beck, B. J., Sherman, D. H., and Reynolds, K. A. (2002) Biochemical evidence for an editing role of thioesterase II in the biosynthesis of the polyketide pikromycin. *J. Biol. Chem. 277*, 48028−48034.
(13) Liu, T., Lin, X., Zhou, X., Deng, Z., and Cane, D. E. (2008) Mechanism of thioesterase-catalyzed chain release in the biosynthesis of the polyether antibiotic nanchangmycin. *Chem. Biol. 15*, 449−458.
(14) Yeh, E., Kohli, R. M., Bruner, S. D., and Walsh, C. T. (2004) Type II thioesterase restores activity of a NRPS module stalled with an aminoacyl-S-enzyme that cannot be elongated. *ChemBioChem 5*, 1290−1293.
(15) Koglin, A., Löhr, F., Bernhard, F., Rogov, V. V., Frueh, D. P., Strieter, E. R., Mofid, M. R., Güntert, P., Wagner, G., Walsh, C. T., Marahiel, M. A., and Dötsch, V. (2008) Structural basis for the selectivity of the external thioesterase of the surfactin synthetase. *Nature 454*, 907−911.
(16) Schwarzer, D., Mootz, H. D., Linne, U., and Marahiel, M. A. (2002) Regeneration of misprimed nonribosomal peptide synthetases by type II thioesterases. *Proc. Natl. Acad. Sci. U. S. A. 99*, 14083−14088.
(17) Claxton, H. B., Akey, D. L., Silver, M. K., Admiraal, S. J., and Smith, J. L. (2009) Structure and functional analysis of RifR, the type II thioesterase from the rifamycin biosynthetic pathway. *J. Biol. Chem. 284*, 5021−5029.
(18) Whicher, J. R., Florova, G., Sydor, P. K., Singh, R., Alhamadsheh, M., Challis, G. L., Reynolds, K. A., and Smith, J. L. (2011) Structure and function of the RedJ protein, a thioesterase from the prodiginine biosynthetic pathway in Streptomyces coelicolor. *J. Biol. Chem. 286*, 22558−22569.
(19) Guntaka, N. S., Healy, A. R., Crawford, J. M., Herzon, S. B., and Bruner, S. D. (2017) Structure and Functional Analysis of ClbQ, an

Unusual Intermediate-Releasing Thioesterase from the Colibactin Biosynthetic Pathway. *ACS Chem. Biol. 12*, 2598−2608.
(20) Olano, C., Wilkinson, B., Sánchez, C., Moss, S. J., Sheridan, R., Math, V., Weston, A. J., Braña, A. F., Martin, C. J., Oliynyk, M., Méndez, C., Leadlay, P. F., and Salas, J. A. (2004) Biosynthesis of the angiogenesis inhibitor borrelidin by Streptomyces parvulus Tü4055: cluster analysis and assignment of functions. *Chem. Biol. 11*, 87−97.
(21) Hillson, N. J., Rosengarten, R. D., and Keasling, J. D. (2012) j5 DNA assembly design automation software. *ACS Synth. Biol. 1*, 14−21.
(22) Gibson, D. G., Young, L., Chuang, R.-Y., Venter, J. C., Hutchison, C. A., and Smith, H. O. (2009) Enzymatic assembly of DNA molecules up to several hundred kilobases. *Nat. Methods 6*, 343−345.
(23) Quadri, L. E., Weinreb, P. H., Lei, M., Nakano, M. M., Zuber, P., and Walsh, C. T. (1998) Characterization of Sfp, a Bacillus subtilis phosphopantetheinyl transferase for peptidyl carrier protein domains in peptide synthetases. *Biochemistry 37*, 1585−1595.
(24) Classen, S., Hura, G. L., Holton, J. M., Rambo, R. P., Rodic, I., McGuire, P. J., Dyer, K., Hammel, M., Meigs, G., Frankel, K. A., and Tainer, J. A. (2013) Implementation and performance of SIBYLS: a dual endstation small-angle X-ray scattering and macromolecular crystallography beamline at the Advanced Light Source. *J. Appl. Crystallogr. 46*, 1−13.
(25) Dyer, K. N., Hammel, M., Rambo, R. P., Tsutakawa, S. E., Rodic, I., Classen, S., Tainer, J. A., and Hura, G. L. (2014) High-throughput SAXS for the characterization of biomolecules in solution: a practical approach. *Methods Mol. Biol. 1091*, 245−258.
(26) Hura, G. L., Menon, A. L., Hammel, M., Rambo, R. P., Poole, F. L., Tsutakawa, S. E., Jenney, F. E., Classen, S., Frankel, K. A., Hopkins, R. C., Yang, S.-J., Scott, J. W., Dillard, B. D., Adams, M. W. W., and Tainer, J. A. (2009) Robust, high-throughput solution structural analyses by small angle X-ray scattering (SAXS). *Nat. Methods 6*, 606−612.
(27) Rambo, R. P., and Tainer, J. A. (2013) Accurate assessment of mass, models and resolution by small-angle scattering. *Nature 496*, 477−481.
(28) Schneidman-Duhovny, D., Hammel, M., Tainer, J. A., and Sali, A. (2013) Accurate SAXS profile computation and its assessment by contrast variation experiments. *Biophys. J. 105*, 962−974.
(29) Schneidman-Duhovny, D., Hammel, M., Tainer, J. A., and Sali, A. (2016) FoXS, FoXSDock and MultiFoXS: Single-state and multi-state structural modeling of proteins and their complexes based on SAXS profiles. *Nucleic Acids Res. 44*, W424−W429.
(30) Jancarik, J., and Kim, S. H. (1991) Sparse matrix sampling: a screening method for crystallization of proteins. *J. Appl. Crystallogr. 24*, 409−411.
(31) Pereira, J. H., McAndrew, R. P., Tomaleri, G. P., and Adams, P. D. (2017) Berkeley Screen: a set of 96 solutions for general macromolecular crystallization. *J. Appl. Crystallogr. 50*, 1352−1358.
(32) Winter, G., Lobley, C. M. C., and Prince, S. M. (2013) Decision making in xia2. *Acta Crystallogr., Sect. D: Biol. Crystallogr. 69*, 1260−1273.
(33) McCoy, A. J., Grosse-Kunstleve, R. W., Adams, P. D., Winn, M. D., Storoni, L. C., and Read, R. J. (2007) Phaser crystallographic software. *J. Appl. Crystallogr. 40*, 658−674.
(34) Adams, P. D., Afonine, P. V., Bunkóczi, G., Chen, V. B., Davis, I. W., Echols, N., Headd, J. J., Hung, L.-W., Kapral, G. J., Grosse-Kunstleve, R. W., McCoy, A. J., Moriarty, N. W., Oeffner, R., Read, R. J., Richardson, D. C., Richardson, J. S., Terwilliger, T. C., and Zwart, P. H. (2010) PHENIX: a comprehensive Python-based system for macromolecular structure solution. *Acta Crystallogr., Sect. D: Biol. Crystallogr. 66*, 213−221.
(35) Afonine, P. V., Grosse-Kunstleve, R. W., Echols, N., Headd, J. J., Moriarty, N. W., Mustyakimov, M., Terwilliger, T. C., Urzhumtsev, A., Zwart, P. H., and Adams, P. D. (2012) Towards automated crystallographic structure refinement with phenix.refine. *Acta Crystallogr., Sect. D: Biol. Crystallogr. 68*, 352−367.
(36) Emsley, P., and Cowtan, K. (2004) Coot: model-building tools for molecular graphics. *Acta Crystallogr., Sect. D: Biol. Crystallogr. 60*, 2126−2132.
(37) Davis, I. W., Leaver-Fay, A., Chen, V. B., Block, J. N., Kapral, G. J., Wang, X., Murray, L. W., Arendall, W. B., Snoeyink, J., Richardson, J. S., and Richardson, D. C. (2007) MolProbity: all-atom contacts and structure validation for proteins and nucleic acids. *Nucleic Acids Res. 35*, W375−W383.
(38) Cantu, D. C., Chen, Y., and Reilly, P. J. (2010) Thioesterases: a new perspective based on their primary and tertiary structures. *Protein Sci. 19*, 1281−1295.
(39) Kapust, R. B., and Waugh, D. S. (1999) Escherichia coli maltose-binding protein is uncommonly effective at promoting the solubility of polypeptides to which it is fused. *Protein Sci. 8*, 1668−1674.
(40) Franke, J., and Hertweck, C. (2016) Biomimetic thioesters as probes for enzymatic assembly lines: synthesis, applications, and challenges. *Cell Chemical Biology 23*, 1179−1192.
(41) Ellman, G. L. (1958) A colorimetric method for determining low concentrations of mercaptans. *Arch. Biochem. Biophys. 74*, 443−450.
(42) Ollis, D. L., Cheah, E., Cygler, M., Dijkstra, B., Frolow, F., Franken, S. M., Harel, M., Remington, S. J., Silman, I., Schrag, J., Sussman, J. L., Verschueren, K. H. G., and Goldman, A. (1992) The α/β hydrolase fold. *Protein Eng., Des. Sel. 5*, 197−211.
(43) Tsai, S. C., Miercke, L. J., Krucinski, J., Gokhale, R., Chen, J. C., Foster, P. G., Cane, D. E., Khosla, C., and Stroud, R. M. (2001) Crystal structure of the macrocycle-forming thioesterase domain of the erythromycin polyketide synthase: versatility from a unique substrate channel. *Proc. Natl. Acad. Sci. U. S. A. 98*, 14808−14813.
(44) Nardini, M., and Dijkstra, B. W. (1999) α/β Hydrolase fold enzymes: the family keeps growing. *Curr. Opin. Struct. Biol. 9*, 732−737.
(45) Bruner, S. D., Weber, T., Kohli, R. M., Schwarzer, D., Marahiel, M. A., Walsh, C. T., and Stubbs, M. T. (2002) Structural basis for the cyclization of the lipopeptide antibiotic surfactin by the thioesterase domain SrfTE. *Structure 10*, 301−310.
(46) Korman, T. P., Crawford, J. M., Labonte, J. W., Newman, A. G., Wong, J., Townsend, C. A., and Tsai, S.-C. (2010) Structure and function of an iterative polyketide synthase thioesterase domain catalyzing Claisen cyclization in aflatoxin biosynthesis. *Proc. Natl. Acad. Sci. U. S. A. 107*, 6246−6251.
(47) Tsai, S.-C., Lu, H., Cane, D. E., Khosla, C., and Stroud, R. M. (2002) Insights into channel architecture and substrate specificity from crystal structures of two macrocycle-forming thioesterases of modular polyketide synthases. *Biochemistry 41*, 12598−12606.
(48) Zhang, W., Chakravarty, B., Zheng, F., Gu, Z., Wu, H., Mao, J., Wakil, S. J., and Quiocho, F. A. (2011) Crystal structure of FAS thioesterase domain with polyunsaturated fatty acyl adduct and inhibition by dihomo-gamma-linolenic acid. *Proc. Natl. Acad. Sci. U. S. A. 108*, 15757−15762.
(49) Giraldes, J. W., Akey, D. L., Kittendorf, J. D., Sherman, D. H., Smith, J. L., and Fecik, R. A. (2006) Structural and mechanistic insights into polyketide macrolactonization from polyketide-based affinity labels. *Nat. Chem. Biol. 2*, 531−536.
(50) Frueh, D. P., Arthanari, H., Koglin, A., Vosburg, D. A., Bennett, A. E., Walsh, C. T., and Wagner, G. (2008) Dynamic thiolation-thioesterase structure of a non-ribosomal peptide synthetase. *Nature 454*, 903−906.
(51) Liu, Y., Zheng, T., and Bruner, S. D. (2011) Structural basis for phosphopantetheinyl carrier domain interactions in the terminal module of nonribosomal peptide synthetases. *Chem. Biol. 18*, 1482−1488.
(52) Huguenin-Dezot, N., Alonzo, D. A., Heberlig, G. W., Mahesh, M., Nguyen, D. P., Dornan, M. H., Boddy, C. N., Schmeing, T. M., and Chin, J. W. (2019) Trapping biosynthetic acyl-enzyme intermediates with encoded 2,3-diaminopropionic acid. *Nature 565*, 112−117.

https://dx.doi.org/10.1021/acs.biochem.0c00126
Biochemistry 2020, 59, 1630−1639

(53) Barajas, J. F., Blake-Hedges, J. M., Bailey, C. B., Curran, S., and Keasling, J. D. (2017) Engineered polyketides: Synergy between protein and host level engineering. *Synthetic and Systems Biotechnology 2*, 147−166.
(54) Ziesack, M., Rollins, N., Shah, A., Dusel, B., Webster, G., Silver, P. A., and Way, J. C. (2018) Chimeric Fatty Acyl-Acyl Carrier Protein Thioesterases Provide Mechanistic Insight into Enzyme Specificity and Expression. *Appl. Environ. Microbiol. 84*, e02868-17.
(55) Jochens, H., Hesseler, M., Stiba, K., Padhi, S. K., Kazlauskas, R. J., and Bornscheuer, U. T. (2011) Protein engineering of α/β-hydrolase fold enzymes. *ChemBioChem 12*, 1508−1517.
(56) Bayly, C. L., and Yadav, V. G. (2017) Towards precision engineering of canonical polyketide synthase domains: recent advances and future prospects. *Molecules 22*, 235−253.
(57) Chakravarty, B., Gu, Z., Chirala, S. S., Wakil, S. J., and Quiocho, F. A. (2004) Human fatty acid synthase: structure and substrate selectivity of the thioesterase domain. *Proc. Natl. Acad. Sci. U. S. A. 101*, 15567−15572.
(58) Wang, M., and Boddy, C. N. (2008) Examining the role of hydrogen bonding interactions in the substrate specificity for the loading step of polyketide synthase thioesterase domains. *Biochemistry 47*, 11793−11803.
(59) Chen, X.-P., Shi, T., Wang, X.-L., Wang, J., Chen, Q., Bai, L., and Zhao, Y.-L. (2016) Theoretical Studies on the Mechanism of Thioesterase-Catalyzed Macrocyclization in Erythromycin Biosynthesis. *ACS Catal. 6*, 4369−4378.
(60) Hari, T. P. A., Labana, P., Boileau, M., and Boddy, C. N. (2014) An evolutionary model encompassing substrate specificity and reactivity of type I polyketide synthase thioesterases. *ChemBioChem 15*, 2656−2661.

https://dx.doi.org/10.1021/acs.biochem.0c00126
Biochemistry 2020, 59, 1630−1639